Flight Dynamics Modeling for a Rapid Conceptual Development Environment

Troy A. Abraham*
Utah State University, Logan, UT, 84322

Casey L. Denham†
NASA Langley Research Center, Hampton, VA, 23681

This paper presents the integration of flight dynamics modeling (FDM) within an aircraft conceptual development framework. Within this framework, FDM and simulation are used for the preliminary analysis of the takeoff, landing, and critical loss of thrust performance of early-stage aircraft concepts. The aerodynamic and propulsive models are built using the XML-based DAVE-ML model exchange. Automated integration of these models is achieved using the Simulink® model generation available through the DAVEtools Java package in addition to Simulink®-based flight simulation blocks. Results demonstrating the established methods are presented for the analysis of a twin-engine light transport example aircraft. This work establishes methods that will be used to perform trade studies of aircraft designed for Regional Air Mobility operations. These aircraft will require short takeoff and landing distances in addition to steep climb and descent gradients, each of which can be estimated and applied as design space constraints using the current methods.

I. Introduction

The integration of flight dynamics modeling (FDM) within an aircraft conceptual development framework enables the simulation of critical flight phases, which can be used to inform early-stage design decisions. The current work demonstrates the development and implementation of FDM and flight simulation tools for the analysis of Normal Category Airplanes, as defined under 14 CFR Part 23 [1], during takeoff, landing, and trimmed flight following a critical loss of thrust (CLOT) scenario. These simulation results can be used as point performance checks for concept feasibility as aircraft design parameters—including mass properties, wing and control surface sizing, and propulsion system characteristics— are modified [2]. These simulations can further narrow the design space beyond simple weight, range, and efficiency metrics and allow concept certifiability to be considered at an earlier stage in the design process.

Within this work, certifiability is evaluated through concept performance relative to the 14 CFR Part 23 requirements [1]. Examples are provided to demonstrate the use of the FDM and simulation tools in determining metrics such as the distance required for ground roll, takeoff, 50 ft obstacle clearance, and landing. Additionally, results are presented concerning a critical loss of thrust, which often determines the size of an aircraft's control surfaces [3, 4]. The automation of these analyses is achieved using simple control systems, which allow for repeatability and integration of these methods within a larger design space toolset.

A major challenge of implementing FDM and simulation in the early conceptual design stage is the general lack of data characterizing the aerodynamic and mass properties of immature designs. Mass property estimates and models of the aircraft aerodynamics, propulsion system, and control system are necessary for full six degree-of-freedom (6-DOF) simulation. The current work is integrated within an existing framework designed to quickly generate the data necessary to develop many of these models.

A. Rapid Conceptual Development Environment

Aircraft design involves information from numerous disciplines including geometry, aerodynamics, propulsion, structures, weights, stability, and control. In the earliest stages of aircraft design, specifically the conceptual design phase, much of the information pertaining to an aircraft is still unknown. The conceptual design phase is where the first analyses and calculations for an aircraft are performed. Fundamental design decisions occur at this design stage that

*PhD Candidate, Mechanical and Aerospace Engineering Dept., 4130 Old Main Hill, AIAA Member.
†Aerospace Technologist - Aerospace Vehicle Design and Mission Analysis, Aeronautics Systems Analysis Branch, AIAA Member

serve as the foundation upon which the rest of the aircraft project will be built. It is important to not limit the design space for new aircraft concepts and allow the exploration of innovative and unconventional ideas. To this end, it is vital to ensure that the process for conceptual design is flexible enough to analyze a wide range of aircraft concepts, fast enough to analyze a large number of candidate designs, standardized to enable valuable comparisons and easy reproduction of analyses, and inclusive of analyses of appropriate fidelity.

To facilitate this process, a highly integrated and standardized framework for conceptual aircraft design, titled the Rapid Conceptual Development Environment (RapCDE), is under development within the Aeronautics Systems Analysis Branch (ASAB) at NASA Langley Research Center. RapCDE leverages common aircraft design tools found within ASAB and focuses on computational speed with adequate fidelity. This approach enables the analysis of a large number of configurations to ensure that the entire trade space is explored. The end result is an abundance of standardized data that the aircraft configurator can use to make appropriate key design decisions and ensure a viable conceptual aircraft design is selected for further maturation. In its current state, RapCDE incorporates five disciplines—geometry, aerodynamics, weights, battery modeling [5], and a mission component— with plans to incorporate more disciplines in the future. The work being presented in this paper will add the flight dynamics and flight simulation disciplines to the existing RapCDE framework.

B. Aircraft for Regional Air Mobility

The methods established in this work will help enable trade studies of light transport aircraft with mission requirements appropriate for Regional Air Mobility (RAM) operations. RAM aircraft are expected to carry up to 19 passengers, or an equivalent weight in cargo, and will operate out of regional airports with close proximity to established communities [6]. To mitigate noise disturbances to these communities, RAM aircraft will likely require short takeoff and landing distances as well as steep climb and descent gradients. These requirements have motivated the use of an existing light transport aircraft as an example case for the results presented in this work. Future work will extend these studies to full RAM aircraft concepts, which will likely include distributed electric propulsion (DEP) systems to improve their takeoff and landing performance.

The remainder of this work outlines and demonstrates the RapCDE FDM and simulation tools. First, the simulation framework is introduced in Section II, which includes model generation, model integration, and control system design. Results are then presented in Section III for the takeoff, landing, and critical loss of thrust performance of the example light transport aircraft. Finally, this work is concluded with summarizing remarks and a discussion on future work in Section IV.

II. Methods

A. Simulation Framework

This work presents the development and implementation of a fully integrated and automated simulation tool within the RapCDE. Its primary purpose is to analyze the takeoff and landing performance of candidate aircraft as well as their ability to achieve trim following a critical loss of thrust. Results generated using these simulations will be used in comparisons with established requirements and to guide successive design iterations. The information flow between the simulation tools and the RapCDE is depicted in Fig. 1. Process blocks developed for this work are shown in blue and the inputs/outputs are in red. The current work focuses on the development, implementation, and demonstration of the methods within the dashed red box, which includes Simulink®-based FDMs, Simulink®-based 6-DOF flight simulations, and automated flight phase analysis scripts.

Given a set of aircraft sizing and performance requirements—such as passenger count, mission range, and propulsion system type—the tools and models within RapCDE produce estimates for the aerodynamic forces and moments, propulsion system performance, and mass properties of a candidate aircraft. This information is stored as a text-based data dictionary file that is made available to the downstream analyses. A flight dynamics model is automatically generated using the aircraft data dictionary and an extensible markup language (see Subsection II.B). This model is then integrated as an individual subsystem block within the larger Simulink® flight simulation model. Additional components within the Simulink® model have been repurposed from the NASA Generic Transport Model (GTM) simulation work [7], including the 6-DOF equation-of-motion integration block and trim algorithm.

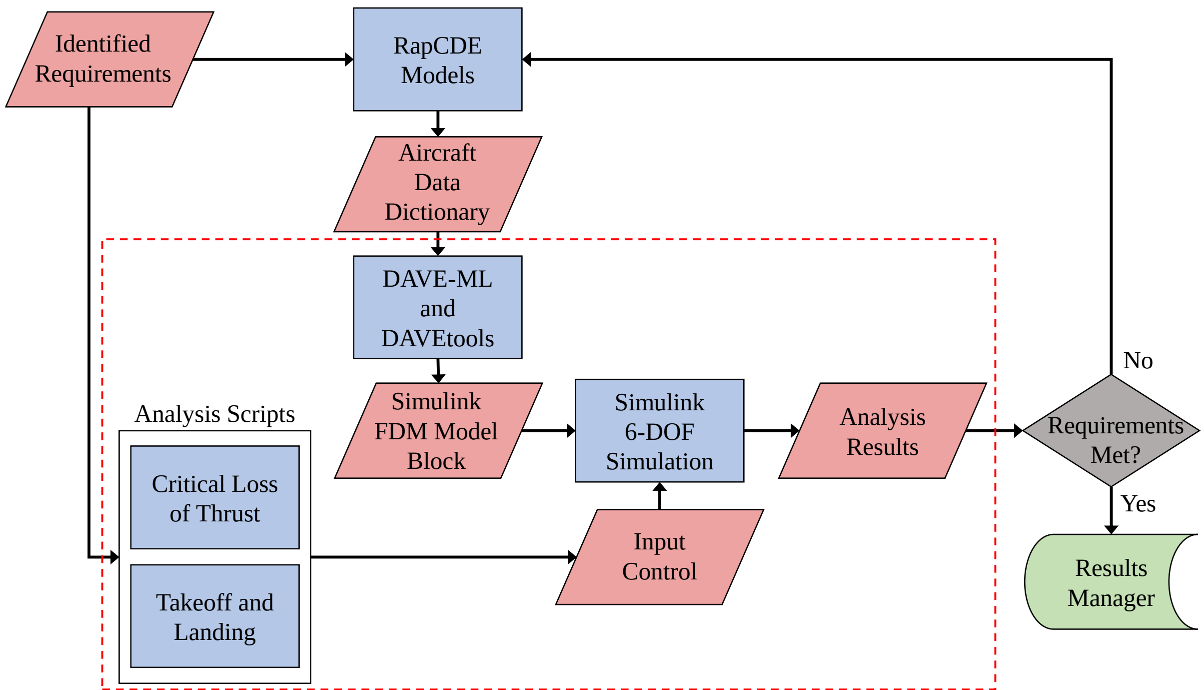

Fig. 1 RapCDE flight dynamics modeling and simulation workflow.

B. DAVE-ML: An Extensible Markup Language (XML) Based Flight Dynamics Model Exchange

The Dynamic Aerospace Vehicle Exchange Markup Language (DAVE-ML) [8] was established as a standard format for defining aerospace vehicle flight dynamics models. Fundamentally, DAVE-ML provides a framework for formatting information in a way that allows easy exchange of models between different simulation and analysis groups that might utilize different software or programming languages. Within DAVE-ML, aerodynamic and propulsion models are built through non-linear function descriptions of either algebraic expressions or tabulated data. The Java-based package DAVEtools provides additional convenience for integrating DAVE-ML within a simulation environment. This work utilizes the DAVE2SL tool specifically, which enables the creation of Simulink® subsystems based on the models defined within a DAVE-ML file.

The current work uses the DAVE-ML gridded table function definitions for modeling aerodynamic coefficients and ungridded table functions for the propulsive system models. The gridded table definitions require a structured dataset and the ungridded tables can be used with unstructured data. This is convenient when working with data generated through different sources, as was the case in this work, where engine data is frequently not calculated for all combinations of altitude, Mach number, and power code setting. The DAVE-ML files are written using a MATLAB® script that automatically converts tabulated aerodynamic data to the required DAVE-ML format. This process enables varying the fidelity and resolution of aerodynamic data points without requiring any additional work from the user to generate an updated DAVE-ML file. The creation of a Simulink® block via DAVEtools, which requires a Java compiling step, and updating that block within the larger Simulink® simulation model is also automated using a MATLAB® script. The process of generating the aerodynamic and propulsion Simulink® blocks via DAVE-ML and DAVEtools is shown in Fig. 2.

C. Aerodynamic, Propulsion, and Mass Properties

The FDM and simulation frameworks have been established in a way that is agnostic to the source of the aerodynamic, propulsion, and mass properties data. By using a standard data dictionary format, the process in Fig. 2 can be integrated with different aircraft analysis toolsets with relative ease. Although the methods for generating these data is an automated process within the larger RapCDE framework, a short description of how these data were obtained in the current paper is provided for clarity.

The aerodynamic force and moment data were generated using the VSPAERO [9] analysis tool distributed with

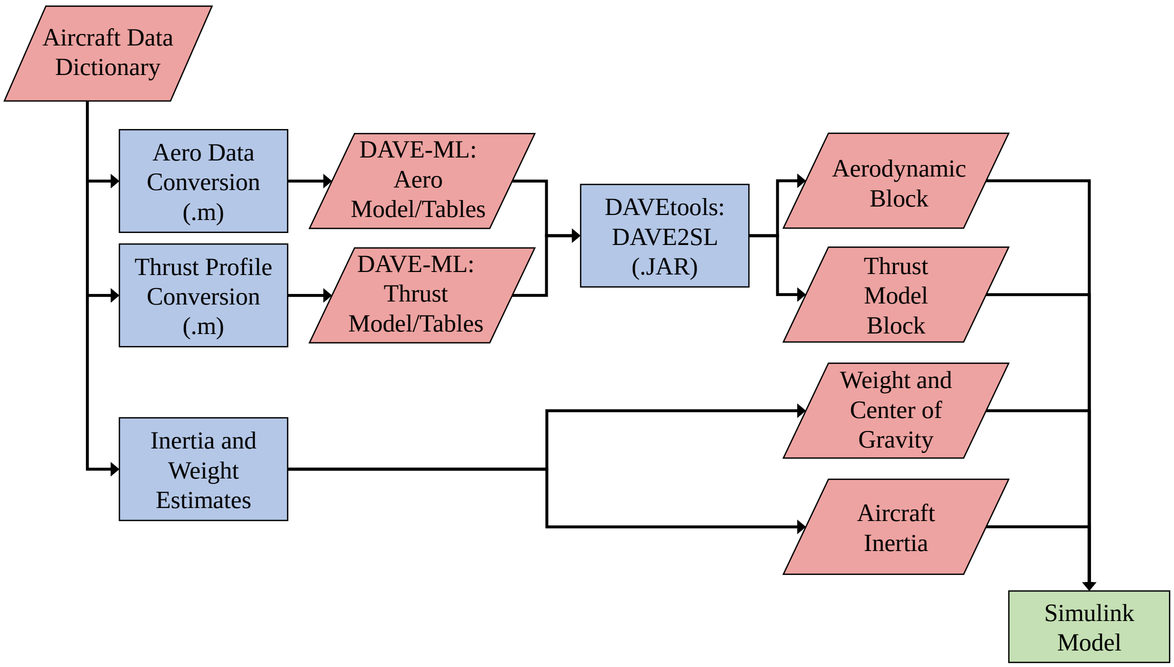

Fig. 2 Process flow from aircraft data dictionary to simulation environment components.

the Open Vehicle Sketch Pad (OpenVSP) software [10]. VSPAERO includes both vortex lattice method (VLM) and panel method solvers that directly utilize aircraft geometries modeled within OpenVSP. In this work, the VLM method was used for inviscid aerodynamic force and moment predictions and the OpenVSP Parasite Drag tool was used for parasitic drag estimates. Additionally, the VSPAERO stability mode analysis was performed to estimate the pitch, roll, and yaw damping derivatives. VSPAERO is well suited for conceptual design work as it can provide good aerodynamic predictions at a relatively low computational cost compared to higher-fidelity methods.

The VSPAERO flow conditions used to sample aerodynamic data in the current work are given in Table 1. The resulting tabulated force and moment estimates were used to build the DAVE-ML-based flight dynamics model through the process shown in Fig. 2. The flight dynamics model used in the current work assumes a linear relationship between the aerodynamic coefficients and the control inputs. Linear extrapolation is used to estimate values outside the flow conditions listed in Table 1. This process represents a minimum proof of concept that will be improved through more efficient data sampling techniques in the future.

Table 1 Flow conditions used to sample aerodynamic data within VSPAERO

Parameter	Values
Angle of attack (α), deg	[-5, 0, 5, 10]
Sideslip angle (β), deg	[-10, 0, 10]
Aileron deflection (δ_a), deg	[-25, 0, 25]
Elevator deflection (δ_e), deg	[-25, 0, 25]
Rudder deflection (δ_r), deg	[-25, 0, 25]
Mach number	[0.1, 0.3]

The propulsion data were parsed from a Flight Optimization System (FLOPS) [11] engine deck file. The engine deck file provides gross thrust and ram drag values at combinations of Mach number, altitude, and power code levels. The mass properties were estimated through a component build up of weight and inertia values using FLOPS and input into OpenVSP [12]. Future work within RapCDE will incorporate automated methods for estimating both the propulsive and mass property data sets of candidate aircraft designs.

D. Control System Design

Simple proportional-integral (PI) control systems were implemented as a proof of concept within the takeoff and landing simulations presented in this work. These control systems were developed to emulate piloted takeoff and landing procedures within the automated simulation-based analyses. A flight path angle controller based on the design presented by Allerton [13] was used for control of the climb angle on takeoff and the glide slope angle on landing, both represented as γ. Figure 3 represents this control system design, which uses the difference in the measured pitch rate, q, and commanded pitch rate, q_c, as the error signal, e_c. The commanded pitch rate is determined using a proportional relationship between the error in flight path angle and the gain value K_1. The elevator deflection angle, δ_e, was used as the control signal. Limiters on both the commanded pitch rate signal and the elevator deflection signal were used to constrain those parameters to physically reasonable values.

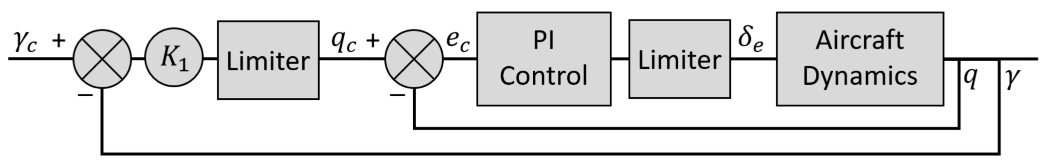

Fig. 3 PI design for glide slope and climb angle control.

The flare path portion of the landing simulations utilized a control system based on the methods outlined in Blakelock [14]. This controller is represented in Fig. 4 and uses the difference in commanded sink rate, $\dot{h}_c$, and measured sink rate, $\dot{h}$, as the error signal and elevator deflection as the control signal.

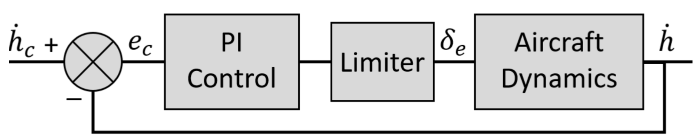

Fig. 4 PI design for flare path control.

The desired flare path is defined using the following exponential relationship for altitude, h_c, as a function of time

$$h_c = h_0 e^{\frac{-t}{\tau}} \tag{1}$$

where τ is a nondimensional time constant and h_0 is the altitude at which the flare path is initiated. Control of the flare path is achieved primarily through the desired number of time constants on the flare path. Differentiation of Eq. (1) results in

$$\dot{h}_c = -\frac{h_0}{\tau} e^{\frac{-t}{\tau}} = -\frac{h_c}{\tau} \tag{2}$$

which is the required sink rate along the flare path, $\dot{h}_c$. The initial rate of descent is related to the glide slope angle and the airspeed of the aircraft, and is defined as

$$\dot{h}_c|_{t=0} = V \sin(\gamma) \tag{3}$$

The altitude at which the flare path is initiated can be derived from Eq. (2) for $t = 0$, which yields

$$h_c|_{t=0} = -\tau \dot{h}_c|_{t=0} = -\tau V \sin(\gamma) \tag{4}$$

Additional single-input single-output control systems were also necessary. Airspeed control was accomplished using a PI controller with an error signal defined as the difference between the measured and desired airspeed and the engine throttle setting as the control signal. Due to the longitudinal/lateral coupling of 6-DOF simulations, a PI controller for bank angle control using the ailerons was necessary to maintain consistent headings during nominal takeoff and landing simulations. Simulations involving a CLOT utilized a yaw rate controller with a rudder deflection control signal. The gains for each of these control systems were tuned manually. Future work within RapCDE will implement updated control methods that will simplify control system design and automate gain tuning.

E. Example Analyses of a Twin-Engine Light Transport Aircraft

Within the RapCDE framework, an aircraft configuration is defined using a set of design variables related to the geometry of the fuselage, wing, and stabilizers. At a minimum, a user is required to specify a subset of variables, which fully define each component. Additional variables can be used to modify detailed aspects of the aircraft's components and add both complexity and variation to the design space. A main wing is defined using a combination of any three of the following variables: aspect ratio, taper ratio, root chord, tip chord, span, and wing area. The horizontal and vertical stabilizers are defined using a wing area and volume coefficient. Examples of additional optional variables for lifting surfaces include sweep and dihedral. The fuselage is defined with either the maximum number of passengers and seats abreast or a length and width. A default value will be assumed for any optional variable that has not been provided as input.

The current work demonstrates the performance of an example twin-engine light transport aircraft defined within the RapCDE framework. The design variables defining this configuration are given in the Appendix. This example is representative of the general size and performance of aircraft expected to be used in future RAM operations. The aircraft takeoff and landing performance is evaluated using MATLAB® scripts to establish the initial conditions, execute the simulations, and record and evaluate the results.

III. Example Analyses

A. Doublet Response

A doublet response of the example aircraft is demonstrated in Fig. 5 as changes to equivalent airspeed (EAS), angle of attack, and sideslip angle. The aircraft simulation was initialized and trimmed in level flight at a 240 ft/s equivalent airspeed cruise condition. The elevator, ailerons, and rudder were deflected at 15, 30, and 45 seconds from the start of the simulation, respectively. The magnitude of each control surface deflection was 4.0 deg and they were each applied for a duration of 0.4 seconds. The longitudinal dynamics of the aircraft are observed as changes to airspeed and angle of attack. The phugoid mode is characterized by the lightly damped oscillations in airspeed and the short period mode is exhibited as the highly damped variations in angle of attack. The lateral dynamics of the aircraft are demonstrated in the changes to slideslip angle. The small sideslip angle perturbations beginning at 30 seconds of simulation time are due to the aileron inputs. The larger sideslip variations beginning at 45 seconds are a result of the rudder input and are indicative of the aircraft's Dutch roll mode. These results demonstrate a working simulation framework and exhibit expected aircraft dynamics, both of which provide confidence in the toolset.

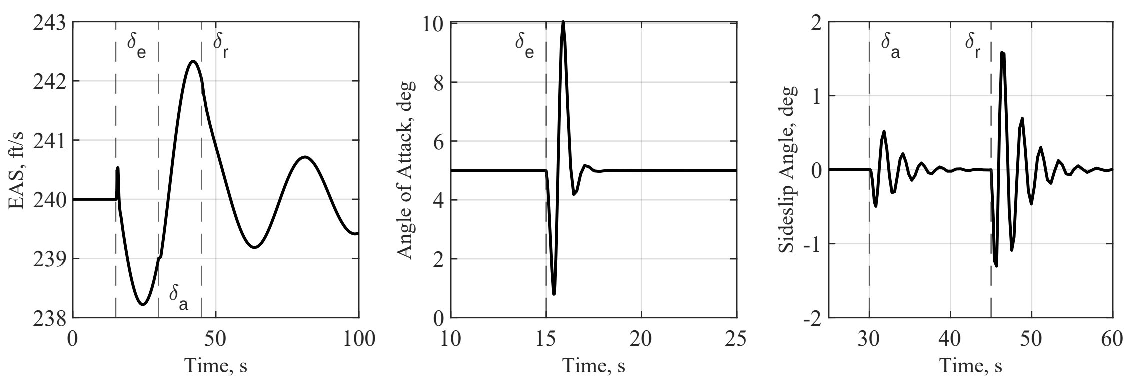

Fig. 5 Example of a doublet response at a 240 ft/s equivalent airspeed cruise condition.

B. Takeoff Performance Simulation

The 14 CFR Part 23 [1] requirements state that all level 3 aircraft must be able to maintain at least a 4% climb gradient, approximately a 2.3 deg climb angle, after takeoff under nominal conditions. Additionally, the distance required for ground roll and 50 ft obstacle clearance must be determined. The RapCDE FDM toolset is used to generate example takeoff results that demonstrate aircraft performance related to these 14 CFR Part 23 requirements. Initialization of this simulation requires the user to specify a rotation airspeed, V_R, and a target climb angle, γ. The throttle setting is initialized and maintained at its maximum value throughout takeoff and climb. Once the simulation is started, the aircraft accelerates through the ground roll phase until the specified rotation speed is achieved. Upon reaching that rotation speed, the climb angle control system (Fig. 3) is enabled and the aircraft attempts to pitch up and climb above the runway altitude. As the aircraft climbs, the control system continues to accelerate the aircraft and attempts to maintain the target climb angle until a user specified flight duration is achieved. Takeoff performance metrics are evaluated using the aircraft state information, which is recorded throughout the duration of the simulation.

Figure 6 shows results demonstrating the takeoff performance of the example aircraft modeled in this work. A rotation airspeed of 147 ft/s and target climb angles of 3.0 deg, 5.0 deg, and 7.0 deg were specified. The rotation airspeed was achieved at a runway distance of approximately 1,800 ft. Liftoff from the runway was achieved at approximately 2,350 ft. The distance at which 50 ft obstacle clearance was achieved varied between the three different solutions, as indicated by the vertical red lines in Fig. 6. The $\gamma = 3.0$ deg solution required approximately 250 ft more distance to reach the 50 ft obstacle clearance altitude than the $\gamma = 7.0$ deg solution. Additionally, the tradeoff between airspeed and climb rate is demonstrated through the variation in altitudes and airspeeds achieved for a given distance traveled. The takeoff safety speed, V_2, of the $\gamma = 3.0$ deg solution was approximately 8.0 ft/s faster than the $\gamma = 7.0$ deg solution. This information can be used to determine a climb profile that both achieves the desired climb rates as well as maintains a V_2 at the required levels above the minimum control airspeed.

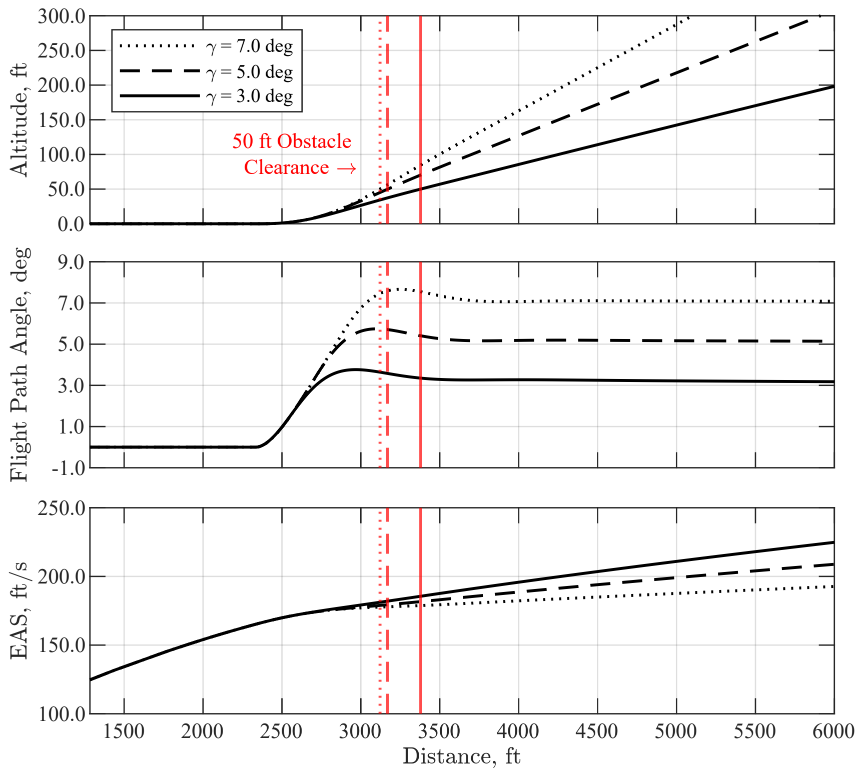

Fig. 6 Example of the RapCDE FDM takeoff simulation results.

These results demonstrate just some of the intended uses of takeoff simulations within the RapCDE framework. Future studies will consider balanced field lengths, optimal takeoff distances, and optimal climb rates for a given configuration. These metrics will be used to evaluate and compare multiple candidate configurations and ultimately narrow the size of the design space.

C. Landing Performance Simulation

This section demonstrates an example landing simulation developed using the RapCDE FDM toolset. This simulation requires the user to specify a target glide slope angle and a reference approach airspeed. Additionally, the number of time steps associated with the exponential flare path, as defined in Eqs. (1) and (2), is required. The simulation is initialized with the aircraft on approach at a target glide slope angle and a specified altitude above the runway. The glide slope control system (Fig. 3) attempts to maintain the target glide slope angle until the initial flare path altitude, defined in Eq. (4), is reached. Once this altitude is attained, the flare path control system (Fig. 4) is enabled and the aircraft attempts to follow the flare path until touchdown is achieved. After touchdown, braking forces are applied to slow the aircraft down until its airspeed reaches zero and the simulation is terminated.

Figure 7 shows results demonstrating the landing performance of the example aircraft. The simulation was initialized at an altitude of 500 ft, a reference airspeed of 172 ft/s, and a glide slope angle of 3.0 deg. Results using flare path time constants, τ, of 2.5, 3.5, and 4.5 are included for comparison. The altitude of flare path initiation for each of the three time constants was 22.5, 31.5, and 40.4 ft, respectively. Note that the distance represented on the x-axis has been adjusted to place the zero value at the point of 50 ft obstacle clearance.

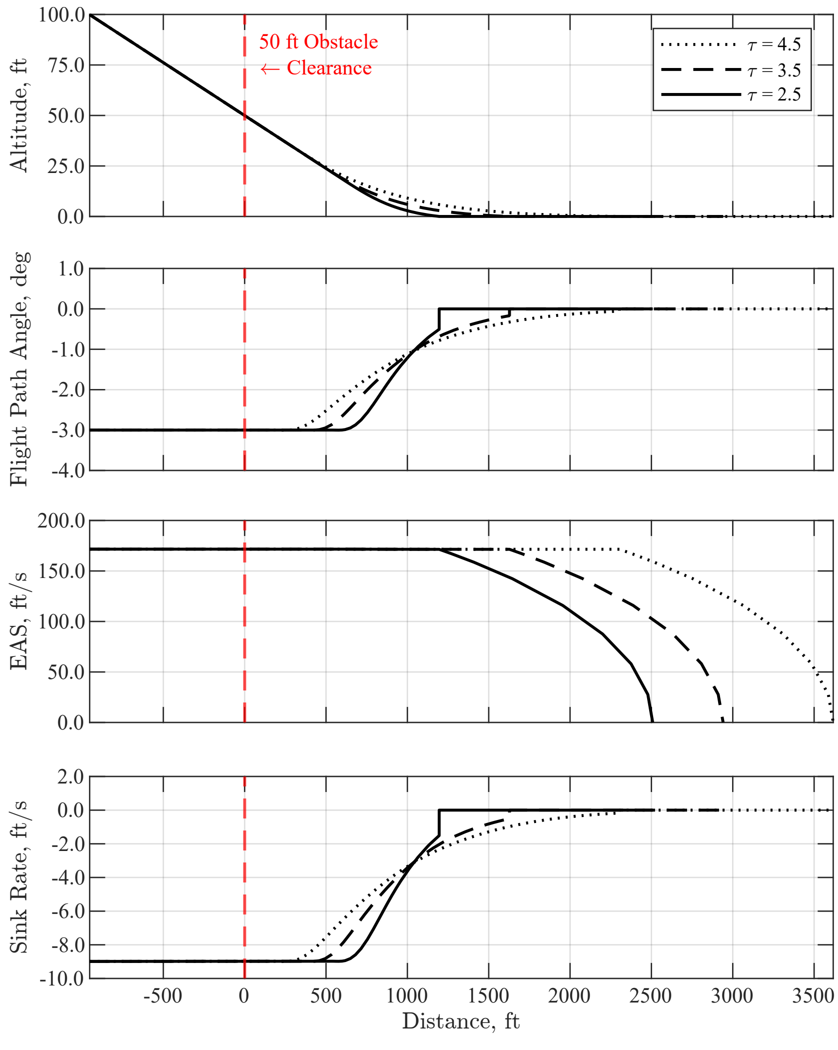

Fig. 7 Example of the RapCDE FDM landing simulation results for three different flare path time constants, τ.

The current airspeed control system maintains airspeed during the glide slope and flare path portions of the simulation. Future work will allow the aircraft to reduce airspeed along the flare path. The landing distance, defined as the distance from 50 ft obstacle clearance to the location of a complete stop [1], varies significantly between the three solutions. The τ = 4.5 solution follows a more shallow flare path and touches down with a 0.2 ft/s sink rate. This results in a landing distance of over 1,100 ft more than the $\tau = 2.5$ solution, which has a 1.5 ft/s sink rate at touchdown. The trade-off between landing distance and vertical speed at touchdown demonstrates just a few of the potential metrics that can be considered in future RapCDE design space studies.

D. Critical Loss of Thrust Trim Solutions

Performance following a critical loss of thrust will play a significant role in identifying candidate Regional Air Mobility aircraft through design space studies. Under 14 CFR Part 23 [1], low-speed level 3 multiengine aircraft are required to maintain at least a 1.0% climb gradient, approximately a 0.57 deg climb angle, following a critical loss of thrust. Additionally, to maintain controlled flight, the control surfaces of the aircraft must be able to offset the moments introduced as a result of the engine failure without exceptional piloting skill [1]. The FDM and simulation tools presented here provide the ability to study aircraft performance following CLOT through trim solutions at different combinations of engine failure and flight phases. Both before and after simulations begin, one or more of the aircraft's engines may be disabled, causing asymmetric thrust and resulting in a nonzero moment about the aircraft's center of gravity.

Table 2 provides a comparison between trim solutions at both nominal and left engine inoperative CLOT conditions. These results were generated for both a $V = 230$ ft/s level flight cruise condition and a $\gamma = 2.0$ deg climb condition with an assumed takeoff safety speed of $V_2 = 158$ ft/s. These flight conditions represent approximate limits in airspeed and climb angle at which the example aircraft was able achieve trim. It should be noted that the throttle settings in these trim solutions represent the value required to maintain airspeed. This differs from the previous takeoff solutions which used a maximum throttle setting throughout the simulation, which better represents current procedures.

Table 2 Comparison of nominal and CLOT trim solutions

		Level Flight, 230 ft/s		Climb, $\gamma = 2.0$ deg, 158 ft/s	
Parameter	**Limits**	**Nominal**	**CLOT**	**Nominal**	**CLOT**
Angle of attack, deg	-	5.44	5.43	11.42	11.40
Aileron deflection, deg	[-25, 25]	-0.04	0.12	-0.09	0.33
Elevator deflection, deg	[-25, 25]	-4.80	-4.74	-8.85	-8.69
Rudder deflection, deg	[-25, 25]	-0.01	-3.84	0.02	-12.43
Throttle setting	[0, 1]	0.48	0.98	0.47	0.96

Both nominal solutions show that the rudder and aileron deflections required for trim are essentially zero, as expected. With a left engine inoperative CLOT, negative rudder deflection is required to negate the negative yawing moment induced through asymmetric thrust. The rudder deflection required in the climbing CLOT condition is over three times that required in the level flight condition. Additionally, the throttle setting is doubled to maintain trim at these airspeeds and nearly reaches its upper limit of 1.0 in both CLOT solutions. Since the CLOT climb requirement (14 CFR Part 23.2120) is often a sizing constraint, it is reasonable to be at or near the control limit [1]. The results presented in Table 2 indicate that the throttle setting, thus available thrust, is the limiting input for this example aircraft. This process demonstrates an approach that could be used for control surface and engine sizing within RapCDE design space studies.

E. Critical Loss of Thrust Takeoff Performance Simulation

After demonstrating sufficient trim for a CLOT climb, a takeoff performance simulation was conducted. For this scenario, a takeoff simulation with a target climb angle of 3.0 deg was initialized, as described in III.B. However, at V_R, the left engine was disabled, creating reduced and asymmetric thrust. To maintain suitable performance, the aircraft must maintain a steady climb gradient while keeping lateral angular rates minimized without exceeding maximum deflection of the control surfaces. Figure 8 shows the takeoff simulation results, demonstrating a successful takeoff with an achieved 3.0 deg climb angle. Distance to clear a 50 ft obstacle is around 3,700 ft, approximately 300 ft greater than the full thrust scenario. The aircraft is unable to maintain the desired airspeed at the target 3.0 deg climb angle. This is seen as the slight reduction of airspeed between the point of rotation and the end of the simulation. Control surface deflections, particularly rudder, were well within the maximum deflection limits, as shown in Fig. 9, where rudder deflection is approximately 15 deg during steady state climb.

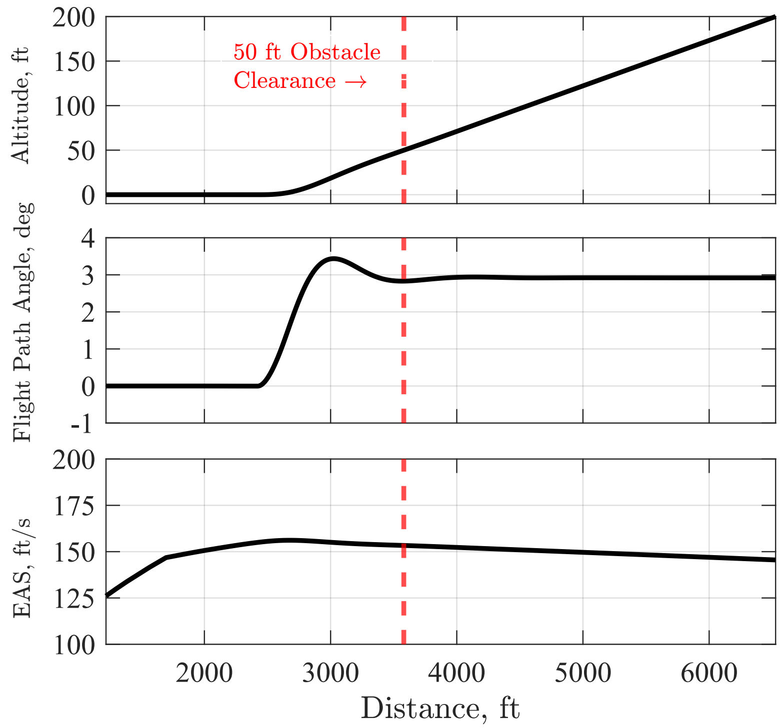

Fig. 8 Example of the RapCDE FDM CLOT takeoff simulation results.

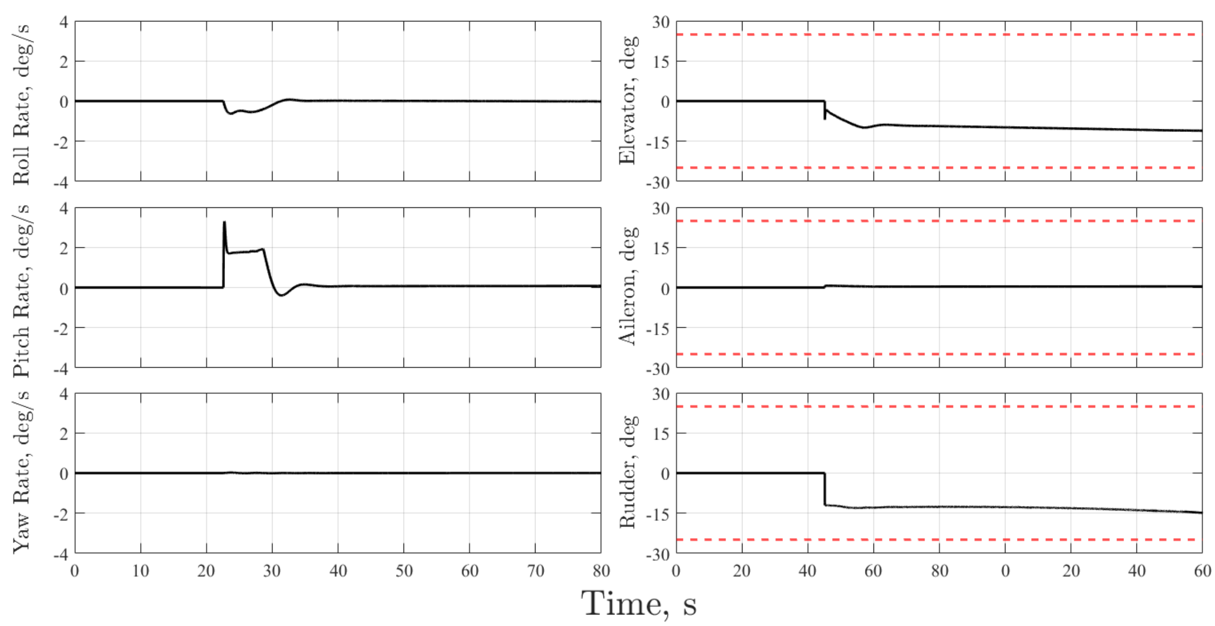

Fig. 9 Example of the RapCDE FDM takeoff simulation results for angular rates and control surface deflections.

IV. Concluding Remarks

This work has considered the integration of flight dynamics modeling within a conceptual aircraft development framework. The goal of this work was to incorporate takeoff, landing, and critical loss of thrust analyses at an early stage of the aircraft design process when information about aircraft configurations is limited and or minimally defined. This ultimately will allow aircraft certification and airworthiness to be considered in identifying candidate aircraft through design space studies. These goals were achieved using the DAVE-ML flight dynamics model exchange, Simulink®-based 6-DOF flight simulation and control systems, and Matlab®-based analysis scripts. These flight dynamics tools were developed as part of the RapCDE toolset within the Aeronautics Systems Analysis Branch at NASA Langley Research Center. The RapCDE toolset will initially be applied to trade studies of light transport aircraft intended for Regional Air Mobility operations. The work presented here used an example twin-engine light transport aircraft that is representative of the size and performance anticipated for RAM operations.

Simulink® model blocks were automatically generated using the aerodynamic, propulsion, and mass properties data provided through the RapCDE toolset. These model blocks were integrated within the Simulink®-based flight simulations and can be updated automatically as aircraft configuration changes are made. Simple proportional-integral (PI) control systems were designed to produce repeatable takeoff and landing simulations with reasonable limits placed on rotation rates and control surface deflections.

Results were presented demonstrating the example aircraft's natural dynamics, takeoff performance, landing performance, and performance during critical loss of thrust. The effects of variations in climb angle following takeoff were seen as differences in climb rate, airspeed, and the distance required for 50 ft obstacle clearance. An additional 250 ft of distance for obstacle clearance was required for a climb angle of 3.0 deg compared to the 7.0 deg solution. A similar set of results was presented for an example landing simulation with varying values for the flare path time constant. Variations in landing distances of over 1,000 ft were seen between solutions for time constants of 2.5 and 4.5. Finally, both nominal and CLOT trim solutions were generated for level cruising flight and climbing flight following takeoff. The trim solutions demonstrated the increase in throttle setting and rudder deflection required to maintain trimmed flight following a critical loss of thrust. Similar results were seen in a CLOT takeoff performance simulation that demonstrated the aircraft's ability to maintain a steady climb gradient following a loss of the left engine. Each of these example analyses demonstrates the information produced using the RapCDE FDM tools that will be useful in identifying candidate aircraft best suited for RAM operations.

Additional work will be required before the FDM methods presented here can be fully implemented and automated within the RapCDE framework. The largest limitation currently is in the method of tuning the control system. The results presented in this work used PI control systems with gains that were tuned manually. Future work will implement updated control methods that will simplify the control system design and automate gain tuning. Methods for identifying maximum climb and descent gradients will also need to be developed. RAM operations will require steep climb and descent gradients and preferred aircraft candidates will not only be able to meet the CFR requirements but rather exceed them.

Appendix

This Appendix outlines the design parameters used to define the example twin-engine light transport aircraft within RapCDE. Table A1 shows the parameters defining the size and geometry of the wing and stabilizers.

Table A1 Lifting surface dimensions

Parameter	Main Wing	Horizontal Tail	Vertical Tail
Planform area, ft^2	225	60	42
Span, ft	44	17	7
Taper ratio	0.60	0.63	0.60

Table A2 details the size of the control surfaces used on each lifting surface. The spanwise length is indicated by a pair of values representing the start and end locations as a percentage of the lifting surface span. The chordwise length of the control surfaces is defined as a percentage of the total chord at the respective spanwise start and end locations.

Table A2 Control surface sizing

Control Surface	% Span start/end	% Chord start/end
Aileron	0.5/0.65	0.3/0.3
Elevator	0.35/0.65	0.3/0.3
Rudder	0.35/0.65	0.3/0.3

The fuselage was defined using the length and width values shown in Table A3, the location and orientation of the two engines are shown in Table A4, and the mass properties of the total aircraft are given in Table A5. Note that the center of gravity location is given relative to the aircraft's nose, which is the origin of the OpenVSP model.

Table A3 Fuselage dimensions

Parameter	Value
Length, ft	33
Width, ft	5

Table A4 Engine properties and position relative to the center of gravity and/or fuselage reference line

Parameter	Value
Body-fixed x offset, ft	7.0
Body-fixed y offset, ft	±8.1
Body-fixed z offset, ft	0
Thrust angle, deg	0
Power, hp	325

Table A5 Aircraft mass properties

Parameter	Value
Weight, lbf	6,885
CG location, ft	[13.6, 0.0, 1.6]
Ixx, slugs-ft^2	9,740
Iyy, slugs-ft^2	5,300
Izz, slugs-ft^2	16,800
Ixy, slugs-ft^2	0
Ixz, slugs-ft^2	524
Iyz, slugs-ft^2	0

The landing gear was modeled using a simple force and moment balance. When the aircraft is in contact with the ground, the normal force resulting from the difference in the weight vector and the sum of the aerodynamic and propulsive force vectors is used to determine a friction force acting opposite the aircraft's direction of motion. Friction coefficients from Raymer [3] were used to represent brakes-off and brakes-on during takeoff and landing simulations, respectively. The friction coefficient values used in this work are summarized in Table A6.

Table A6 Friction coefficients for landing and takeoff simulations

Parameter	Value
Brakes-off	0.03
Brakes-on	0.4

Acknowledgments

This work was completed as part of an internship within the Aeronautics Systems Analysis Branch at the NASA Langley Research Center. The authors thank the Transformational Tools and Technologies project for funding this internship and the Convergence Aeronautics Solutions (CAS) project for providing additional support. Both of these projects are within the Transformative Aeronautics Concepts Program. The authors also thank Nick Borer and Nat Blaesser for their technical guidance and feedback.

References

[1] *Airworthiness Standards: Normal Category Airplanes*, §23.2100 - 23.2130, Federal Aviation Administration, 2023. `https://www.ecfr.gov/current/title-14/chapter-I/subchapter-C/part-23/subpart-B?toc=1` [Accessed 06.11.2024].

[2] Ohme, P., "A Model-Based Approach to Aircraft Takeoff and Landing Performance Assessment," *AIAA Paper 2009–6154*, August 2009. `https://arc.aiaa.org/doi/10.2514/6.2009-6154`.

[3] Raymer, D. P., *Aircraft Design: A Conceptual Approach*, 6th ed., AIAA Education Series, Reston, VA, 2018, Chaps. 4, 17.

[4] Phillips, W. F., *Mechanics of Flight*, 2nd ed., John Wiley & Sons, Inc., Hoboken, NJ, 2010, Chap. 5.

[5] Hallock, T., and Michal, B., "A Higher-Order Battery Model for the Conceptual Design of Electric Aircraft," *AIAA Paper*, August 2024 (not yet published).

[6] Borer, N., Blasesser, N., and Patterson, M., "Regulatory Considerations for Future Regional Air Mobility Aircraft," *AIAA Paper 2023-3294*, June 2023. `https://ntrs.nasa.gov/citations/20230006666`.

[7] Hueschen, R. M., "Development of the Transport Class Model (TCM) Aircraft Simulation From a Sub-Scale Generic Transport Model (GTM) Simulation," NASA TM-2011-217169, 2011. `https://ntrs.nasa.gov/citations/20110014509`.

[8] Jackson, E. B., "Dynamic Aerospace Vehicle Exchange Markup Language (DAVE-ML) Reference," *AIAA Modeling and Simulation Technical Committee*, 2011. `https://daveml.org/`.

[9] Litherland, B., "Using VSPAero," OpenVSP Wiki, 2015. `https://openvsp.org/wiki/doku.php?id=vspaerotutorial#running_vspaero` [Accessed 10.12.2023].

[10] McDonald, R. A., and Gloudemans, J. R., "Open Vehicle Sketch Pad: An Open Source Parametric Geometry and Analysis Tool for Conceptual Aircraft Design," *AIAA Paper 2022-0004*, January 2022. `https://arc.aiaa.org/doi/abs/10.2514/6.2022-0004`.

[11] McCullers, L. A., "Aircraft Configuration Optimization Including Optimized Flight Profiles," *NASA Langley Research Center Recent Experiences in Multidisciplinary Analysis and Optimization NASA CP-2327*, January 1984. `https://ntrs.nasa.gov/citations/19870002310`.

[12] Wells, D. P., Horvath, B. L., and McCullers, L. A., "The Flight Optimization System Weights Estimation Method," NASA TM-2017-219627 Volume I, 2017. `https://ntrs.nasa.gov/citations/20170005851`.

[13] Allerton, D., *Principles of Flight Simulation*, 1st ed., John Wiley & Sons, Inc., Hoboken, NJ, 2009, Chap. 4.

[14] Blakelock, J. H., *Automatic Control of Aircraft and Missiles*, 2nd ed., John Wiley & Sons, Inc., Hoboken, NJ, 1991, Chap. 2.